

**Electronic Supplementary Information for  
Intrinsic Ferromagnetism and Valley Polarization in Hydrogenated Group V  
Transition-metal Dinitride ( $MN_2H_2$ ,  $M = V/Nb/Ta$ ) Nanosheets: Insights from  
First-principles**

Yi Ding<sup>1</sup> and Yanli Wang<sup>2</sup>

<sup>1)</sup>*Department of Physics, Hangzhou Normal University, Hangzhou, Zhejiang 311121,  
Peoples Republic of China.*

<sup>2)</sup>*Department of Physics, Zhejiang Sci-Tech University, Hangzhou, Zhejiang 310018,  
Peoples Republic of China.*

**Contents:**

Figure S1. The AIMD results of  $VN_2H_2$  nanosheets.

Figure S2. The AIMD results of  $TaN_2H_2$  nanosheets.

Figure S3. The exfoliation energies of H- $MN_2H_2$  nanosheets.

Figure S4. The PBE band structures of H- $NbN_2H_2$  multilayers.

Figure S5. The HSE band structures of H- $NbN_2H_2$  multilayers.

Table S1. The Raman and IR active frequencies of H- $NbN_2H_2$  nanosheet.

Table S2. The Raman and IR active frequencies of T- $NbN_2H_2$  nanosheet.

Table S3. The Raman and IR active frequencies of M- $NbN_2H_2$  nanosheet.

Table S4. The Debye temperature of  $MN_2H_2$  nanosheets.

Table S5. The band gaps of semiconducting  $MN_2H_2$  nanosheets.

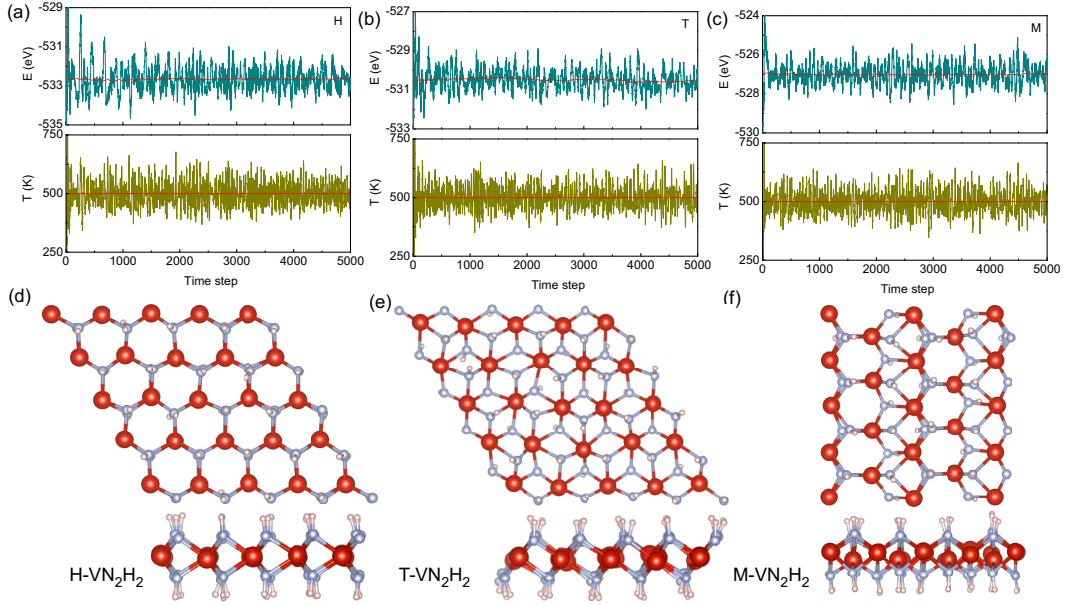


FIG. 1. [(a)-(c)] The total energy and temperature versus time steps for the H-, T-, and M-VN<sub>2</sub>H<sub>2</sub> nanosheets during the AIMD simulations. The dotted lines represent the average values of adjacent data in 1 ps. [(d)-(f)] The snapshots for the final configurations after AIMD simulations.

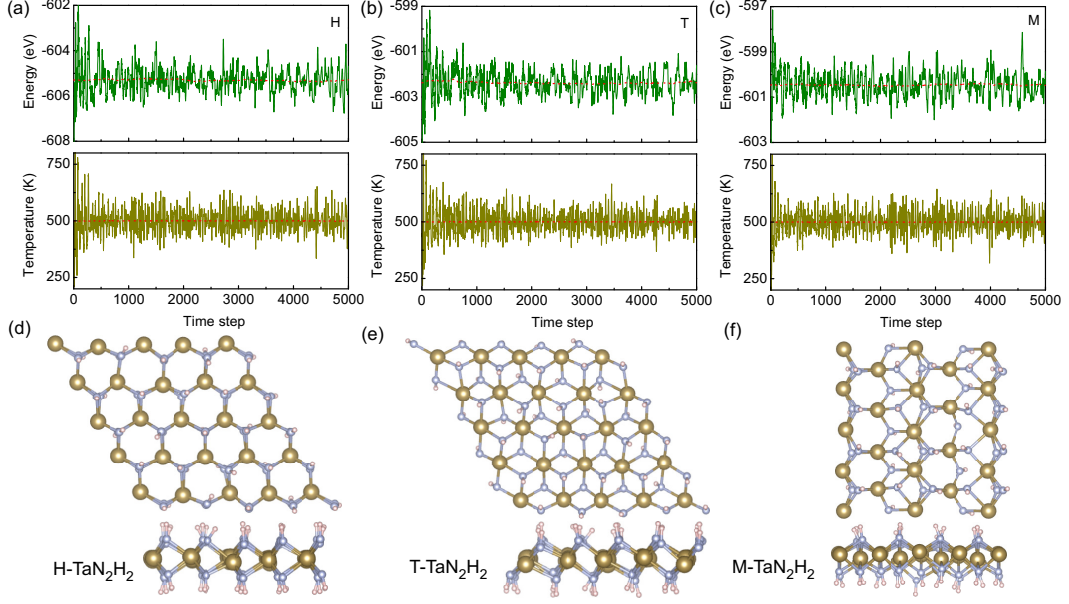


FIG. 2. [(a)-(c)] The total energy and temperature versus time steps for the H-, T-, and M-TaN<sub>2</sub>H<sub>2</sub> nanosheets during the AIMD simulations. The dotted lines represent the average values of adjacent data in 1 ps. [(d)-(f)] The snapshots for the final configurations after AIMD simulations.

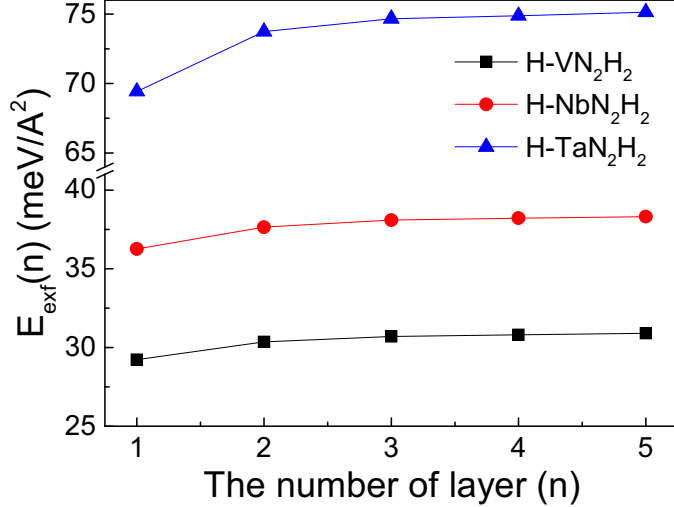


FIG. 3. The  $n$ -layer exfoliation energies ( $E_{exf}(n)$ ) of H-MN<sub>2</sub>H<sub>2</sub> (M=V/Nb/Ta) nanosheets. Here,  $E_{exf}(n)$  is calculated as  $(E_{iso}(n) - E_{bulk} \times n/m)/A$ .  $E_{iso}(n)$  is the unit cell energy of an isolated  $n$ -layer slab structure,  $E_{bulk}$  is the unit cell energy of a bulk material with  $m$  layers, and  $A$  is the in-plane area of the bulk unit cell. For these H-MN<sub>2</sub>H<sub>2</sub> systems, a 2H-NbS<sub>2</sub>-like structure is adopted as their bulk references.

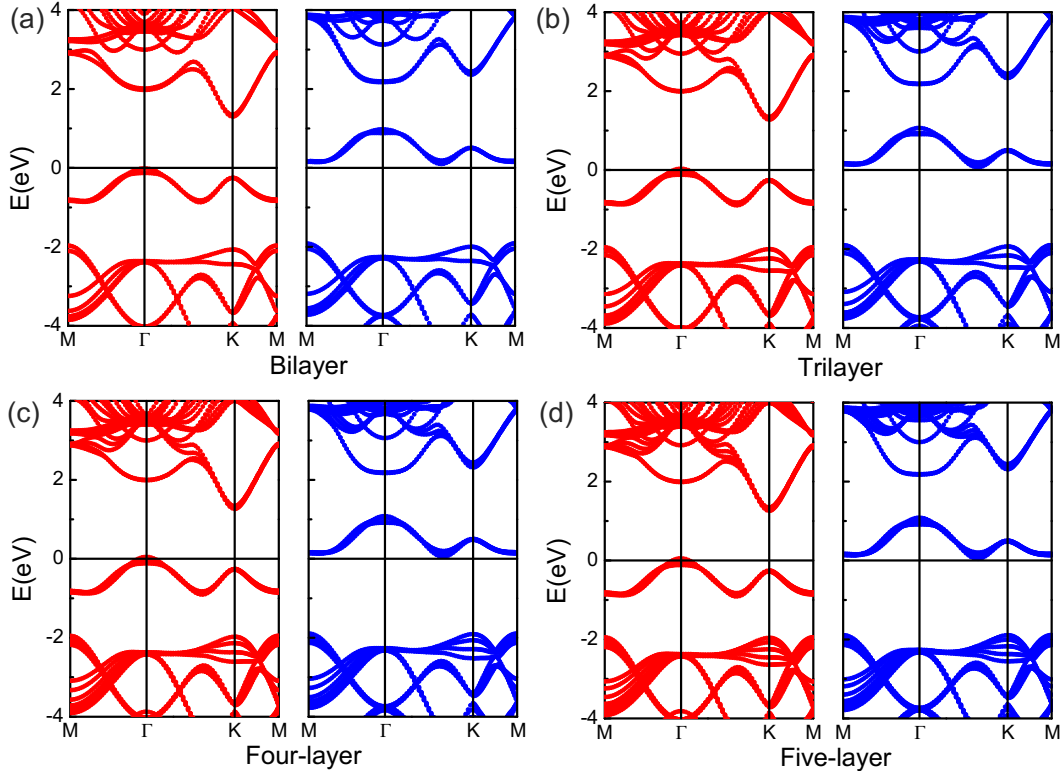


FIG. 4. The PBE band structures of H-NbN<sub>2</sub>H<sub>2</sub> (a) bilayer, (b) trilayer, (c) four-layer, and (d) five-layer systems at the FM state. The corresponding PBE band gaps are 0.12, 0.035 and  $\sim 0$  eV for the bilayer, trilayer, and four-/five-layer ones, which are all smaller than the monolayer case (0.29 eV).

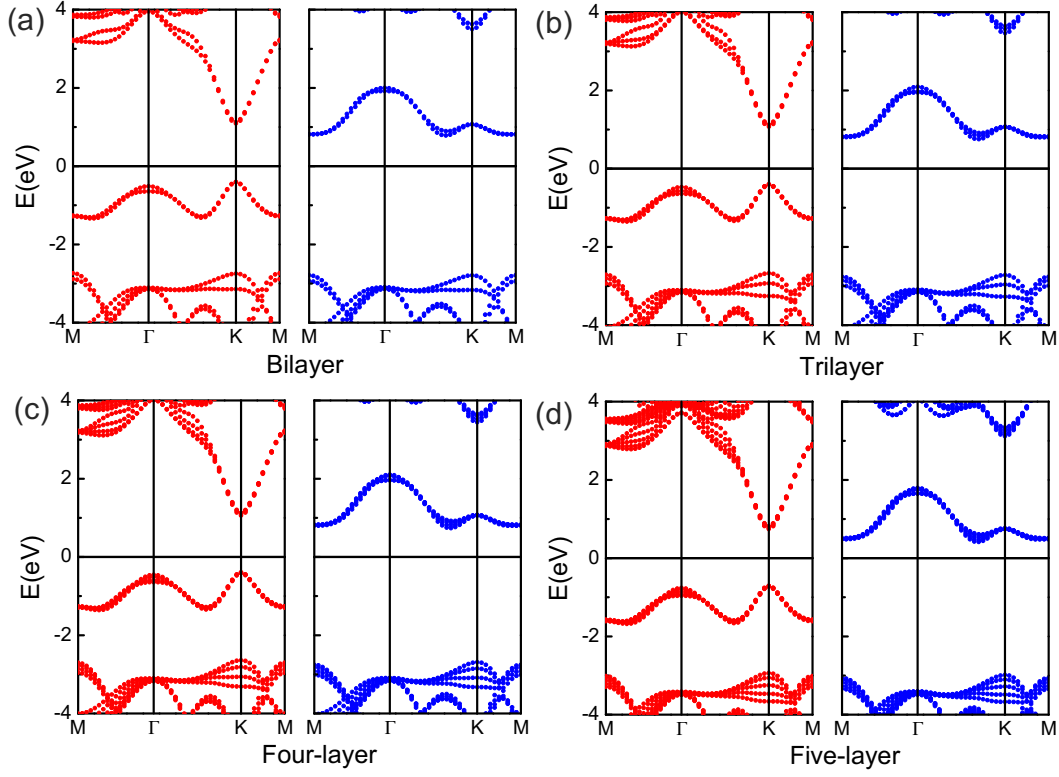


FIG. 5. The HSE band structures of the H-NbN<sub>2</sub>H<sub>2</sub> (a) bilayer, (b) trilayer, (c) four-layer, and (d) five-layer systems at the FM state. The corresponding HSE band gaps are 1.20, 1.15, 1.14 and 1.12 eV for the bilayer, trilayer, four-layer and five-layer ones, which are also smaller than the monolayer case (1.22 eV).

H-NbN <sub>2</sub> H <sub>2</sub>											
Raman	$\omega_1$	$\omega_2$	$\omega_3$	$\omega_4$	$\omega_5$	$\omega_6$	IR	$\omega'_1$	$\omega'_2$	$\omega'_3$	$\omega'_4$
modes	$E''$	$E'$	$A'_1$	$E''$	$E'$	$A'_1$	modes	$E'$	$A_2''$	$E'$	$A_2''$
(cm <sup>-1</sup> )	335	410	653	660	695	3392		410	592	695	3393

TABLE I. The frequencies of the Raman and IR active vibrational modes in the H-NbN<sub>2</sub>H<sub>2</sub> nanosheet.

T-NbN <sub>2</sub> H <sub>2</sub>									
Raman	$\omega_1$	$\omega_2$	$\omega_3$	$\omega_4$	IR	$\omega'_1$	$\omega'_2$	$\omega'_3$	$\omega'_4$
modes	$E_g$	$E_g$	$A_{1g}$	$A_{1g}$	modes	$E_u$	$E_u$	$A_{2u}$	$A_{2u}$
(cm <sup>-1</sup> )	379	533	572	3392		210	533	580	3394

TABLE II. The frequencies of Raman and IR active vibrational modes in the T-NbN<sub>2</sub>H<sub>2</sub> nanosheet.

M-NbN <sub>2</sub> H <sub>2</sub>										
Raman+IR modes	$\omega_1$	$\omega_2$	$\omega_3$	$\omega_4$	$\omega_5$	$\omega_6$	$\omega_7$	$\omega_8$	$\omega_9$	
(cm <sup>-1</sup> )	$A'$	$A''$	$A''$	$A'$	$A'$	$A''$	$A'$	$A''$	$A'$	
	124	153	235	240	320	368	382	408	430	
	$\omega_{10}$	$\omega_{11}$	$\omega_{12}$	$\omega_{13}$	$\omega_{14}$	$\omega_{15}$	$\omega_{16}$	$\omega_{17}$	$\omega_{18}$	
	$A''$	$A'$	$A''$	$A'$	$A'$	$A''$	$A'$	$A'$	$A''$	
	470	475	521	524	580	607	617	652	658	
	$\omega_{19}$	$\omega_{20}$	$\omega_{21}$	$\omega_{22}$	$\omega_{23}$	$\omega_{24}$	$\omega_{25}$	$\omega_{26}$	$\omega_{27}$	
	$A'$	$A'$	$A''$	$A'$	$A'$	$A'$	$A'$	$A'$	$A'$	
	670	691	715	783	799	3325	3412	3422	3442	

TABLE III. The frequencies of Raman and IR active vibrational modes in the M-NbN<sub>2</sub>H<sub>2</sub> nanosheet.

$\theta_D$ (K)	H-phase	T-phase	M-phase
VN <sub>2</sub> H <sub>2</sub>	376	248	262
NbN <sub>2</sub> H <sub>2</sub>	261	173	198
TaN <sub>2</sub> H <sub>2</sub>	199	139	155

TABLE IV. The Debye temperature of MN<sub>2</sub>H<sub>2</sub> nanosheets. Here, the Debye temperature ( $\theta_D$ ) is estimated from the phonon bands as  $\frac{1}{\theta_D^3} = \frac{1}{3}(\frac{1}{\theta_{FA}^3} + \frac{1}{\theta_{TA}^3} + \frac{1}{\theta_{LA}^3})$ , where  $\theta_{FA}/\theta_{TA}/\theta_{LA}$  is obtained from the highest frequency of flexural acoustic (FA)/transverse acoustic (TA)/longitudinal acoustic (LA) phonon branches as  $\theta = \hbar\omega_{max}/k_B$  ( $\hbar$  and  $k_B$  are the Planck constant and Boltzmann constant, respectively).

	VN <sub>2</sub> H <sub>2</sub>			NbN <sub>2</sub> H <sub>2</sub>			Ta <sub>N</sub> <sub>2</sub> H <sub>2</sub>		
(eV)	H	T	M	H	T	M	H	T	M
PBE	0.73	0.09	metal	0.32	metal	0.12	0.15	metal	0.21
PBE+ <i>soc</i>	0.72	0.07	metal	0.27	metal	0.09	0.05	metal	0.13
HSE	2.01	1.50	metal	1.22	0.39	0.91	0.96	metal	0.97
HSE+ <i>soc</i>	1.99	1.50	metal	1.17	0.39	0.89	0.88	metal	0.86

TABLE V. The band gaps of H-, T- and M-MN<sub>2</sub>H<sub>2</sub> (M=V/Nb/Ta) nanosheets by the PBE, PBE+*soc*, HSE and HSE+*soc* calculations.